# Anthropogenic influence on recent severe autumn fire weather in the west coast of the United States

Linnia R Hawkins[1], John T Abatzoglou[2], Sihan Li[3], and David E. Rupp[4]

[1]Forest Ecosystems & Society, Oregon State University
[2]University of California Merced
[3]University of Oxford
[4]Oregon State University

November 21, 2022

**Abstract**

Extreme wind-driven autumn wildfires are hazardous to life and property, due to their rapid rate of spread. Recent catastrophic autumn wildfires in the western United States co-occurred with record- or near-record autumn fire weather indices that are a byproduct of extreme fuel dryness and strong offshore dry winds. Here, we use a formal, probabilistic, extreme event attribution analysis to investigate anthropogenic influence on recent extreme autumn fire weather events. We show that while present-day anthropogenic climate change has slightly decreased the prevalence of strong offshore downslope winds, it has increased the likelihood of extreme fire weather indices by 40%, primarily through increased autumn fuel aridity and warmer temperatures during dry wind events. These findings illustrate that anthropogenic climate change is exacerbating autumn fire weather extremes that contribute to high-impact catastrophic fires in populated regions of the western US.

# Anthropogenic influence on recent severe autumn fire weather in the west coast of the United States

Linnia R. Hawkins[1], John T. Abatzoglou[2], Sihan Li[3,4], David E. Rupp[5]

[1]Forest Ecosystems & Society, Oregon State University, Corvallis, OR, USA

[2]Management of Complex Systems, University of California, Merced, Merced, CA, USA

[3]Environmental Change Institute, School of Geography and the Environment, University of Oxford, Oxford, UK

[4]Oxford e-Research Centre, University of Oxford, Oxford, UK,

[5]Oregon Climate Change Research Institute, College of Earth, Ocean, and Atmospheric Science, Oregon State University, Corvallis, OR, USA

Corresponding author: Linnia Hawkins (Linnia.Hawkins@oregonstate.edu)

## Key Points:

- Anthropogenic climate change has already increased the likelihood of autumn wind-driven extreme fire weather conditions in the western US.
- Increased autumn fuel aridity and warmer temperatures during dry wind events increased the likelihood of extreme fire weather in 2017 and 2018 indices by 40%.
- Present-day anthropogenic climate change has slightly decreased the prevalence of strong offshore downslope winds.

## Abstract

Extreme wind-driven autumn wildfires are hazardous to life and property, due to their rapid rate of spread. Recent catastrophic autumn wildfires in the western United States co-occurred with record- or near-record autumn fire weather indices that are a byproduct of extreme fuel dryness and strong offshore dry winds. Here, we use a formal, probabilistic, extreme event attribution analysis to investigate anthropogenic influence on extreme autumn fire weather events in 2017 and 2018. We show that while present-day anthropogenic climate change has slightly decreased the prevalence of strong offshore downslope winds, it has increased the likelihood of extreme fire weather indices by 40% in areas where recent autumn wind-driven fires have occurred in northern California and Oregon. The increase was primarily through increased autumn fuel aridity and warmer temperatures during dry wind events. These findings illustrate that anthropogenic climate change is exacerbating autumn fire weather extremes that contribute to high-impact catastrophic fires in populated regions of the western US.

## Plain Language Summary

Over the last several years, California and western Oregon have seen their largest and most destructive wildfires on record. The rapid and extensive growth of many of these fires that invaded populated areas was driven by strong, dry, offshore, downslope autumn winds over fuels that had become exceedingly dry over the summer and remained dry into autumn. We used simulations of both the modern-era climate and a climate that could have been, absent human influence, to investigate the effect of anthropogenic climate change on the likelihood of extreme fire weather conditions (warm, very dry, and very windy) that were present during recent catosphrophic wildfires. Despite a small decrease in the frequency of strong offshore winds, anthropogenic climate change has already increased the likelihood of extreme autumn fire weather across most of the west coast of the US through higher temperature and drier fuels, heightening the risk to life and property.

# 1 Introduction

Widespread increases in burned area over the past half-century are evident across the western United States (US) despite decreases in the number of ignitions (Bowman et al., 2020; Keeley and Syphard 2018). Several factors are suspected to have contributed to long-term increases in fire activity including the legacy of aggressive and successful fire suppression that has increased aboveground biomass (Rogers et al., 2020), increased human settlement in fire prone lands (Syphard et al., 2007), and climate change that increases fuel dryness and extends the fire season length (e.g., Abatzoglou and Williams, 2016). Extreme wildfires often occur during fire weather extremes (Stavros et al., 2014). This is particularly true in autumn in California and the Pacific Northwest US as a byproduct of chronically dry fuels prior to the onset of the rain season, which creates a flammable landscape, and strong offshore, downslope winds that drive rapid rates of fire spread (Williams et al., 2019; Nauslar et al., 2018). For example, the 2020 Labor Day fires in western Oregon spread rapidly under conditions of near record downslope winds and near record-breaking fire weather (Abatzoglou et al., 2021a).

Studies have documented increases in autumn fire weather indices and the number of high fire danger days over the past four decades in California (e.g., Goss et al., 2020; Khorshidi et al., 2020). While such changes are consistent with anthropogenic climate change (ACC), statistically rare wind-driven fire weather extremes that have been linked with recent catastrophic fires present a potentially more tenuous link to human-caused climate change given they are a function of both thermodynamic and dynamic elements (National Academy of Sciences, 2016). Whereas the thermodynamics effects of ACC through fuel drying and increased vapor pressure deficit are more straightforward, the dynamic effects of ACC associated with winds are less clear (Williams et al. 2019). For example, studies on projected changes in offshore Santa Ana winds of southwestern California provide contradictory results (Miller and Schlegel 2006; Hughes et al. 2011; Yue et al., 2014; Jin et al., 2015), though recent studies indicate projected attenuation of Santa Ana winds in autumn despite that the ACC influence has been nominal to date (Guzman-Morales and Gershunov 2019; Wang et al., 2020). However, the existing literature does not address the influence of ACC on autumn offshore winds elsewhere in California and western Oregon, nor the relative contribution of ACC via thermodynamic and dynamic effects on rare wind-driven fire weather extremes that may occur once every couple decades.

The science of extreme event attribution has experienced major advances over the last decade and helps provide context for characterizing climate and weather extremes (National Academy of Science, 2016; Bellprat et al., 2019; Uhe et al. 2021). It has, however, been used sparingly for wildfire although some studies exist for individual fire seasons (Kirchmeier-Young et al., 2019; van Oldenborgh et al., 2021) and individual fire events (Tan et al., 2018). While attribution of wildfire is confounded by multiple complementary factors associated with human influence, isolating the influence of ACC in top-down atmospheric factors that enable and drive extreme fires addresses a key aspect of fire risk. Here, we use this attribution framework to determine if, and by how much, ACC has altered the probability of the rare extreme wind-driven fire weather conditions during autumn, similar to conditions observed during several recent high-impact fires in California and Oregon. We specifically focus on offshore wind-driven autumn fire weather conditions from southwestern California to western Washington as such fires can comprise a majority of burned area in a given year (Kolden and Abatzoglou, 2018), are often co-located with human settlement (Jin et al., 2015), and have been associated with secondary impacts such as downstream air quality and de-energization of electrical grid (Aguilera et al., 2021; Abatzoglou et al., 2020).

Here we examine how ACC altered the likelihood of extreme autumn fire weather experienced across the western US using large ensembles of regional climate model simulations. We further decompose the influence of ACC on the likelihood of the individual components contributing to fire weather indices. Additionally, we examine the role of offshore wind events and the influence of ACC on the frequency of such events.

# 2 Methods

## 2.1 Wind driven fires

We examine representative regions in the western US where recent large fires have occurred and were driven by strong offshore winds such as Santa Ana and Diablo winds of California (Jin et al., 2015; Kolden and Abatzoglou, 2018; Keeley and Syphard, 2019) and East winds of western Oregon (Abatzoglou et al., 2021a). Within these regions, we focus on several recent large catastrophic offshore wind-driven autumn wildfires with widespread impacts on communities including the Wine Country Fires in October 2017, the Camp fire in November 2018, and North Complex Glass fires in September 2020 (all in Northern California), the Woolsey fire in November 2018 in Southern California, and the Lionshead fire in September 2020 in western Oregon. These fires provide archetypes of extreme offshore wind-driven autumn fires and guide an objective set of criteria for attribution analyses. To characterize the meteorological conditions associated with each fire relative to a long-term record (1979-2020), a suite of fire weather metrics were calculated using daily meteorological data from gridMET (Abatzoglou, 2013) at the centroid of each fire (Figure 1).

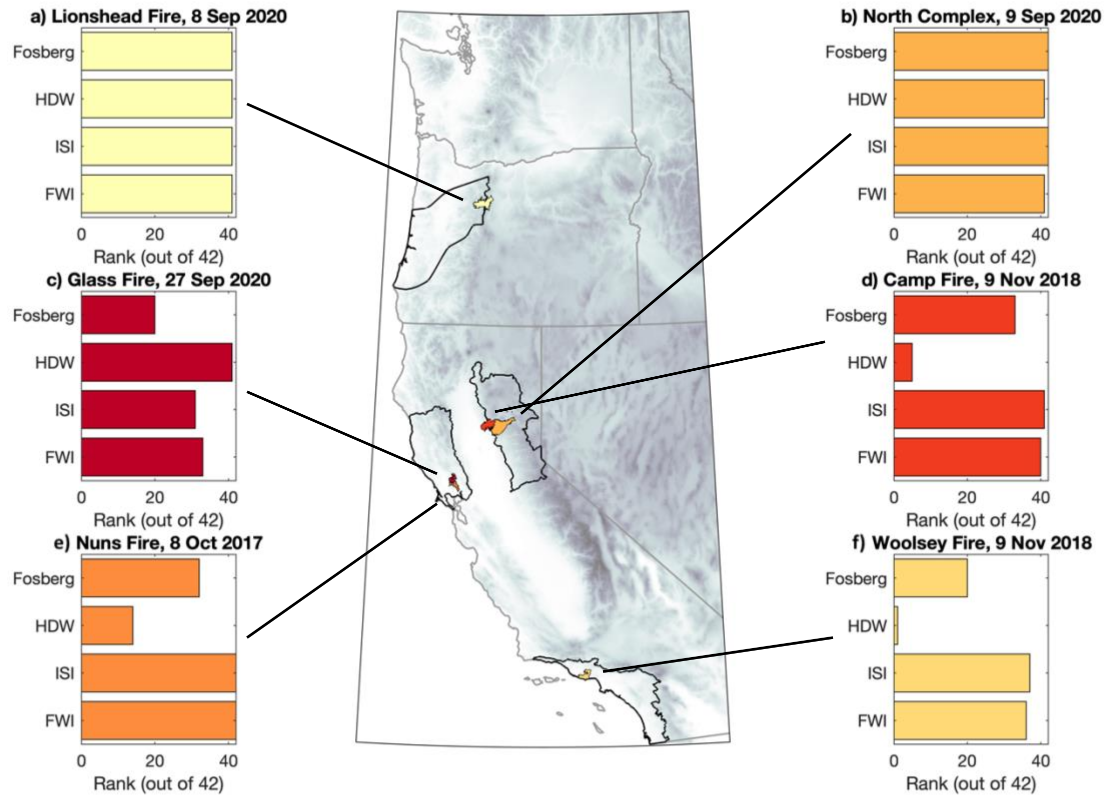


**Figure 1.** Recent significant offshore wind-driven wildfires in the western US. Inset map shows fire perimeters with gray illustrating elevation and black polygons showing the corresponding Predictive Service Areas. Ranked fire weather variables for each fire event are shown for the higher value on either the discovery date or day after, for the Fosberg Fire Weather Index (Fosberg), the Hot-Dry-Windy Index (HDW), the Initial Spread Index (ISI) and the Fire Weather Index (FWI). Variables are ranked from smallest to largest relative to local September-November maximum daily values during 1979-2020.

## 2.2 Climate simulations

Climate simulations were generated through the volunteer computing platform Weather@home (Guilliod et al., 2017; Mote et al., 2016). Our configuration of Weather@home nests the Hadley Centre Regional Climate Model (HadRM3P) at 0.22° × 0.22° horizontal resolution in the Hadley Centre Atmospheric Model (HadAM3P) with updated global and regional model parameters (Hawkins et al., 2019; Li et al., 2019).

We used two large initial condition ensembles of simulations. The first represents modern-era climate conditions (actualClim) that uses observed concentrations of greenhouse gases, aerosols, and observed sea surface temperatures (SSTs; Donlon et al., 2012) for September 2016 through December 2018. The second ensemble represents the climate that would have been without human influence (naturalClim) over the same time period using pre-industrial concentrations of greenhouse gases and aerosols, and observed SST's with the anthropogenic signal removed (Schaller et al., 2014; Uhe et al., 2016). Each large ensemble consists of 1000 simulations of September 2016 through December 2018, generated by perturbing the initial potential temperature field of each ensemble member. We excluded the first year as additional model spinup and use 2,000 realizations of autumn weather (September through November (SON), 2017 and 2018) for analysis. Model outputs consisted of daily (precipitation) or instantaneous values (near-surface wind speed (WS), temperature (TA), relative humidity (RH)) at 21Z (1300 LST) corresponding to the approximate times used in the daily fire danger rating systems. Similar, smaller ensembles (402 actualClim and 1,008 naturalClim realizations) were generated with additional diagnostics to examine prevalence of offshore downslope winds using 21Z wind velocity, temperature, geopotential height at various pressure levels. See Section S1 for additional detail.

### 2.3 Fire weather indices

We calculated three fire weather indices influenced by wind speed and associated with difficulty in fire containment and potential rates of spread given the nature of these wind-driven fires: (1) the fire weather index (FWI) from the Canadian Forest Fire Danger Rating system (Van Wagner, 1987), (2) the Hot-Dry-Windy (HDW) index (Srock et al., 2018), and (3) the Fosberg fire weather index (FFWI; Fosberg, 1978). Notably, FFWI and HDW do not consider fuel moisture or antecedent conditions. Furthermore, we considered two subcomponents of the FWI as diagnostics: the initial spread index (ISI) and the build-up index (BUI). The ISI weakly considers antecedent information through fine fuel moisture content and is strongly influenced by wind speed while the BUI is a measure of longer-term antecedent build-up of fuel drying that does account for the combined influence of temperature, humidity, and precipitation but excludes the influence of wind speed. Finally, we included vapor pressure deficit (VPD) given that it has been shown to be the leading control of fire activity in California (Chen et al., 2021) and observed increases in VPD during autumn have increased the number of high fire potential days in California (Williams et al., 2019). We consider this suite of fire weather metrics given their different formulations, sensitivities to meteorological inputs, and role of antecedent conditions in the resultant metric.

### 2.4 Attribution

We estimated the change in likelihood of extreme fire weather metrics attributable to ACC by comparing the frequency of occurrence of extremes between the actualClim and naturalClim ensembles. We specifically examined all extreme fire weather metrics and associated meteorological variables (temperature, relative humidity, windspeed, and VPD) corresponding to the day of the maximum FWI ($FWI_{max}$) in SON of each simulation year. This harmonization allows us to focus on the most extreme autumn fire weather conditions each year as defined by the widely used FWI, rather than disparate days from different metrics which impedes inter-metric comparisons.

Extreme fire weather conditions were defined as the gridcell 95$^{th}$ percentile of autumn maximum daily FWI in the naturalClim ensemble, i.e., 1-in-20 year autumn event under pre-industrial climate conditions. This threshold was based on the magnitude of fire weather extremes coincident with the recent representative fires (see Section 3.1 below). Similarly, we defined gridcell extremes in other fire weather indices or meteorological variables using the same protocol. We defined the risk ratio as in the $P_{actual}/P_{natural}$ where $P_{actual}$ and $P_{natural}$ are the probabilities of the extreme event occurring in the actualClim ensemble and the naturalClim ensemble respectively. A risk ratio of two means that the 1-in-20 year event is two times more likely to occur in the actualClim ensemble than in the naturalClim ensemble. We estimated confidence intervals for the risk ratio by bootstrap using $n$ =10,000 iterations and sampling ensemble members with replacement. Changes were considered statistically significantly where the 95% confidence interval excluded zero. For regional analyses, we calculated the risk ratio for each grid cell then averaged over the four Predictive Service Area (PSA) boundaries – a management unit used by the US fire agencies – covering regions with recent large wind-driven fires (Figure 1).

### 2.5 Winds

We explicitly examined anthropogenic-forced changes in offshore downslope winds to accompany the fire weather analyses. Due to increased complexity relative to the fire weather index analysis, we limited the spatial extent to regions with well-known offshore downslope winds focusing on East winds along the Oregon Cascades, Diablo winds along the Sierras of northern California, and Santa Ana winds in the Transverse Range of southern California.

We adapted the method of Abatzoglou et al. (2021b) to identify conditions suitable for offshore, downslope winds based on the cross-barrier 700-hPa horizontal wind speed $u \geq 13$ m s$^{-1}$ and the 700-hPa vertical wind speed $\omega \geq 0.6$ Pa s$^{-1}$. We added the criterion that near-surface relative humidity ≤ 30% (e.g., Edinger et al., 1964; Smith et al., 2018) to constrain wind events to those that yield elevated fire weather potential (for more detail, see Section S2). We found that HadRM3p showed credible winds and downslope wind climatologies to those seen with ECMWF ReAnalysis 5 (ERA5; Hersbach et al. 2020) including extremes similar to those present in recent major wildfires (see Section S2-S3; Figures S1-S6). We calculated the change in SON frequency of offshore, downslope wind conditions between the naturalClim and actualClim ensembles for each region and investigated if an ACC signal could be detected on near-surface meteorological variables (VPD, RH, and WS), conditional on the presence of these conditions. Note that unlike our fire weather index analysis focused on very-rare extremes, the analyses of winds considered all offshore downslope winds, rather than 1-in-20 year events.

## 3 Results

### 3.1 Extreme fire weather

Each of the six representative downslope wind-driven autumn fires occurred during fire weather extremes (Figure 1). All fire events had at least one fire weather index that ranked in the 95th percentile for autumn maximum daily values between 1979 and 2020 (40$^{th}$ out of 42 years), including several that coincided with the most extreme autumn fire weather metrics on record.

We found that ACC increased the frequency of autumn fire weather extremes across portions of the western US (Figure 2) relative to pre-industrial levels (Figure S7). Extreme $FWI_{max}$ were, on average, 40% more likely due to ACC across the western US (regional mean risk ratio of 1.40) with significant increases detected across 65% of the domain including along the west coast of Washington, Oregon and northern California, although notably not in southern coastal California (Table S1). In simulations where the $FWI_{max}$ was above the 95$^{th}$ percentile, the regional average temperature was 1.15°C warmer in the actualClim ensemble than in the naturalClim ensemble (Table S2). Similarly, the relative humidity was 0.1% higher, the VPD was 1.52hPa higher, and the wind speed was 0.17m/s lower in the actualClim ensemble, averaged over the domain.

Large increases in the frequency of extreme BUI and HDW were detected across the region (Figure 2c,d), whereas changes in the FFWI index were not significant (Figure 2e). Differences in the response of ACC across fire weather metrics are posited to be a consequence of the sensitivity of each metric to simulated changes in climate. For example, the HDW index is highly sensitive to VPD, which has increased in SON across the western US (Ficklin et al., 2017), and increased significantly on extreme $FWI_{max}$ days in actualClim simulations (Table S1; Figure S8). Similarly, increased temperature coincident with $FWI_{max}$ days in the actualClim simulations facilitates an increase in fire weather indices absent changes in wind speed itself. By contrast, the FFWI is most sensitive to wind speed and relative humidity, and only weakly sensitive to temperature. No significant decreases in any of the fire weather indices were detected within the domain.

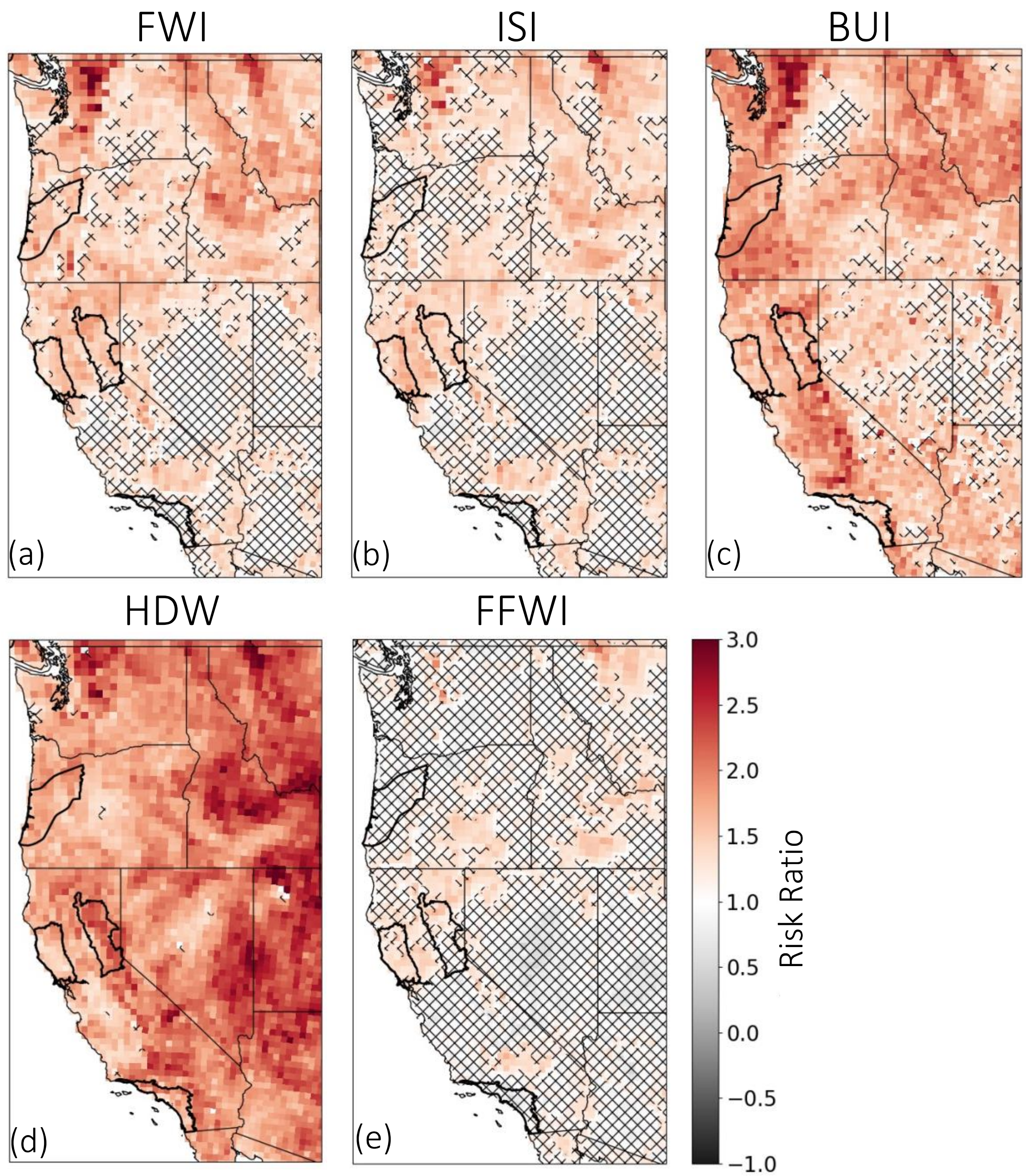


**Figure 2.** Simulated risk ratio of extreme autumn fire weather metrics in modern-era simluations relative to preindustrial simulations. Hatching represents regions where changes

were not significant in bootstrapped 95% confidence intervals. PSA regions are outlined in black.

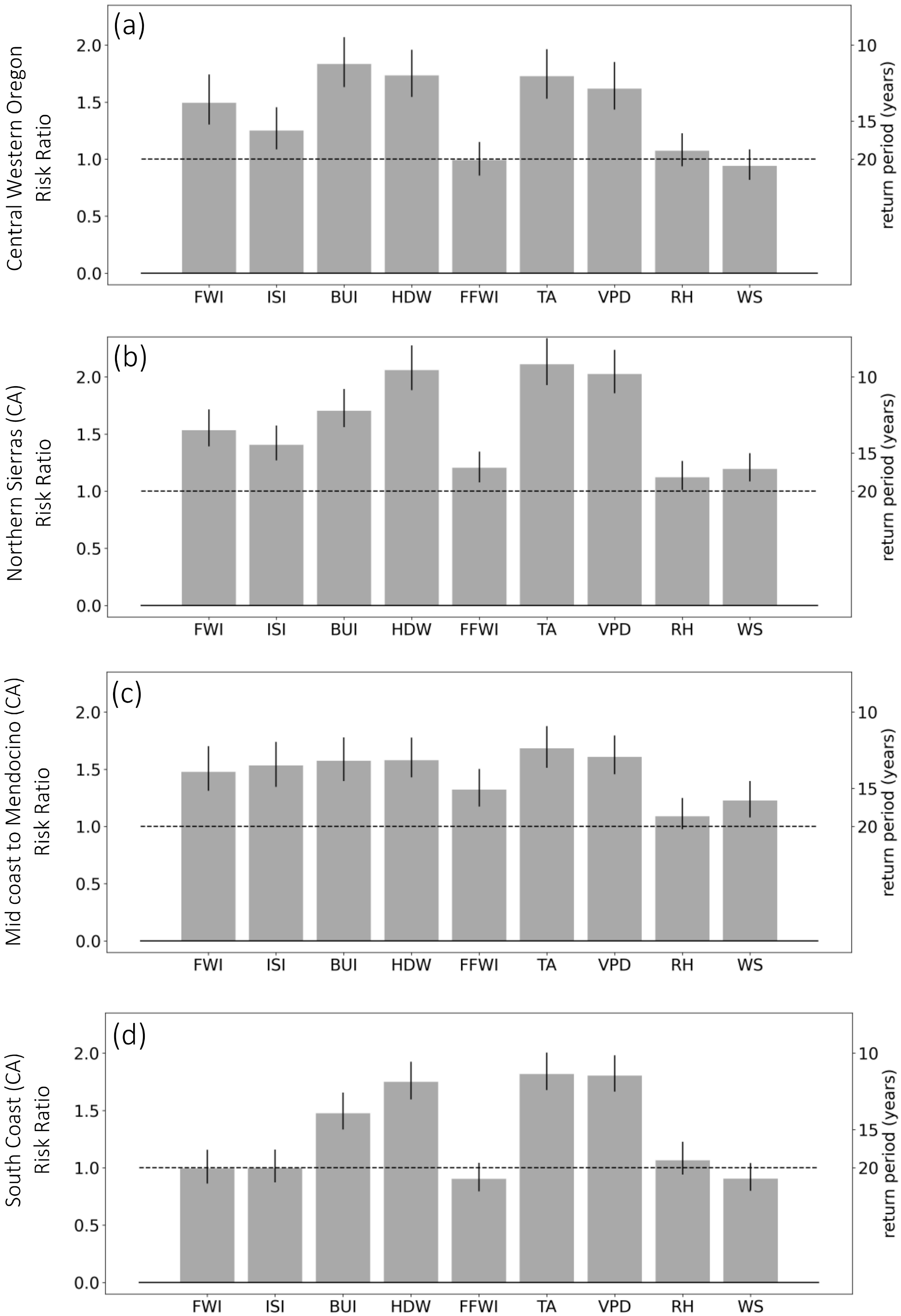


**Figure 3.** Risk ratio of maximum autumn fire weather metrics above the naturalClim 95th percentile (1-in-20 year return interval) in modern-era climate simulations relative to

preindustrial simulations for the Central Western Oregon (a), North Sierras (b), Mid Coast to Mendocino (c), and South Coast (d) PSA regions (depicted in Figure 1) with bootstrapped 95% confidence intervals. Right hand axes show the return period (years) in the actualClim ensemble corresponding to the naturalClim 1-in-20 year event. Horizontal dashed line represents no change in risk.

The risk ratio of extreme fire weather varied among the four PSA regions (Figure 3). In the Central Western Oregon region, ACC increased the risk of extreme $FWI_{max}$ by 49% (risk ratio of 1.49). This increase was most strongly linked to increases in fuel dryness which manifest through the BUI, with smaller contributions from ISI. On days when $FWI_{max}$ occurs, the risk ratio of temperature and VPD were 1.72 and 1.61, respectively. The increase in VPD influenced the risk of extreme HDW, which increased by 73% despite slight decrease in the likelihood of extreme wind speed.

In PSA regions in northern California all fire weather metrics (excluding relative humidity) showed significant increases in the likelihood of extremes. In the northern Sierra region, the risk ratio of the HDW index was 2.06. This indicates that ACC has made extreme autumn HDW conditions twice as likely, i.e., ACC has made a 1-in-20 year HDW event a 1-in-10 year event. The increase in likelihood is primarily driven by an increase in aridity rather than a change in wind speed.

Along the southern California coast we did not detect a significant increase in the frequency of FWI, ISI, or FFWI. This is primarily due to the slight decline in extreme wind speed during extreme fire weather days in this region. The South Coast PSA region did show an increase in aridity with risk ratios extreme temperature and VPD of 1.82 and 1.80, respectively. The increase in aridity lead to detectable increases in the risk of extreme BUI and HDW which had risk ratios of 1.48 and 1.75, respectively. Notably, the influence of BUI on FWI extremes in southern California was negligible given the region's exceptionally long dry season and formulation of the index which make changes in FWI extremes more sensitive to changes in ISI when the BUI is high.

## 3.2 Offshore winds analysis

Offshore, downslope wind frequency decreased from the naturalClim to the actualClim scenario in all regions (Figure 4b; Table S3), though the only statistically robust decrease was seen in Santa Ana wind frequency (region CAd). These results suggest that ACC may already be reducing Santa Ana frequency, consistent with projected changes under global warming through the 21st century (Guzman-Morales and Gershunov, 2019; Wang et al., 2020). Similarly, extreme offshore downslope wind frequency decreased in all regions (Table S3). The consistency in the sign of the changes across all regions also suggests that an anthropogenically forced decrease in the prevalence of such offshore downslope winds is a general consequence of ACC across western US mountain ranges and not limited to Santa Ana winds.

When offshore, downslope conditions did occur, VPD was 5 to 9% higher in the actualClim scenario across the six regions (Figure 4c), driven primarily by a 0.8-1.4°C warming (Table S4). Non-significant decreases in relative humidity were found in all regions (Figure 4c). Similarly, during extreme offshore downslope wind conditions temperatures were 0.7-2.4°C warmer in the actualClim scenario (Table S5). Finally, we found no regionally consistent nor statistically significant changes in near-surface wind speed accompanying downslope wind days (Figure 4c).

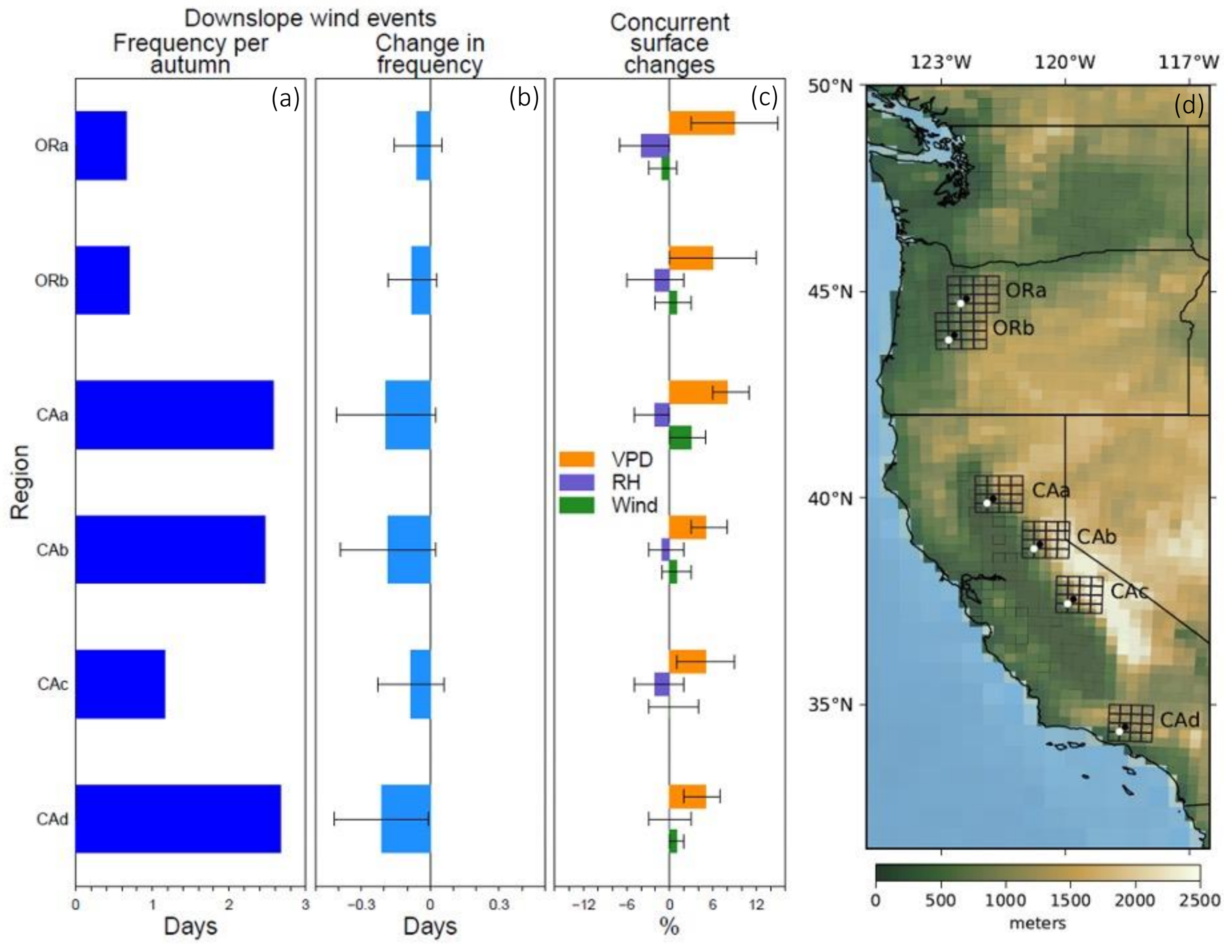


**Figure 4**. Anthropogenic influence on characteristics of autumn (September through November) downslope wind events at 21Z by region. **(a)** Simulated ensemble mean frequency of downslope wind events under modern era forcing (circa 2018); **(b)** change in frequency of events from preindustrial to modern era forcing; **(c)** relative change from preindustrial to modern era forcing in 2-m vapor pressure deficit (VPD), 2-m relative humidity (RH), and 10-m wind speed (Wind) during downslope wind events; **(d)** surface elevation map of the west coast US showing the regions analyzed. The highlighted 4 x 4 grids show the cells used to identify cross-barrier and downward winds at 700 hPa. The black and white circles mark the locations where 10-m winds (black) and 2-m VPD and RH (white) were extracted.

# 4 Discussion and Conclusions

Our regional modeling experiment demonstrates that human-caused climate change substantially increased the likelihood of extreme fire weather metrics in 2017 and 2018 that have been linked with recent catastrophic wind-driven autumn fires from California to Oregon. Across several regions that have experienced high-impact autumn wind-driven fires, we estimate that anthropogenic climate change increased the likelihood of fire weather extremes viewed through metrics like FWI and HDW by at least 50% in 2017 and 2018 (Figure 3). Likewise, while the direction of trends in fire weather indices concur with previous studies (e.g., Goss et al., 2020; McEvoy et al., 2020), our findings are unique given that we isolate the anthropogenic influences for extreme fire weather conditions across a host of fire weather indices. By contrast, decreased frequency in autumn dry, offshore, downslope fire-spreading winds appears to be an emergent anthropogenic signal along the western US from southern California to northwest Oregon, expanding on the findings of Guzman-Morales and Gershunov (2019) for southern California. Increased likelihood of autumn fire weather extremes with anthropogenic climate change appears to be primarily driven by thermodynamic responses that facilitate increased fuel aridity and increased VPD and temperature during fire weather extremes.

Attribution science has rarely been applied to wildfire events given the complex interactions among ignitions, land management, and weather conditions. While we stop short of attributing fire behavior characteristics (e.g., fire spread rate, total burned area) to anthropogenic climate change, distillation of changing likelihoods of extreme fire weather aid in overall risk modeling efforts. We note that our findings are specific to the geography, season, and wind-driven fire archetype, and cannot be compared directly to the attribution of extreme summer fire seasons in previous studies (Kirchmeier-Young et al, 2019; Lewis et al., 2020). Observed and projected delayed onset of autumn precipitation in California hasten the potential for compound fuel aridity-offshore wind extremes that yield fire weather extremes (Luković et al., 2021; Swain et al., 2018). We examined the anthropogenic influence on the timing and magnitude of autumn rains but results were inconclusive, compeling further investigation into the interactions between thermodynamic and dynamic drivers of anthropogenic-driven changes in fire weather conditions.

This study demonstrates that anthropogenic climate change has already increased the likelihood of autumn wind-driven extreme fire weather conditions in the western US. In concert with non-climatic factors such as biomass accumulation and enchroachment of settlement in fire-prone lands, this has increased overall fire risk motivating the adoption of fire-adaptation systems that may ameliorate fire potential and are ecologically appropriate for the landscape (e.g., Moritz et al., 2014; Kolden and Henson, 2018). Finally, the approaches used here can guide near-term fire risk assessments towards directing appropriate adaptation efforts, and better elucidate the how different fire typologies are directly influenced by anthropogenic climate change.

**Acknowledgments**

The authors thank David Wallom and Sarah Sparrow for providing support for weather@home. We would also like to thank the Met Office Hadley Centre PRECIS team for their technical and scientific support for the development and application of weather@Home. Finally, we would like to thank all of the volunteers who have donated their computing time to climateprediction.net and weather@home.

**Data Availability Statement**

Postprocessed model simulations and code used in this study are achieved at : https://doi.org/10.5281/zenodo.5161113

Publicly available datasets used in this study were acquired from the following repositories: ERA5: https://cds.climate.copernicus.eu/cdsapp#!/dataset/reanalysis-era5-pressure-levels?tab=overview ;

gridMET: http://thredds.northwestknowledge.net:8080/thredds/reacch_climate_MET_catalog.html;

## References


Abatzoglou, J. T. (2013). Development of gridded surface meteorological data for ecological applications and modelling. *International Journal of Climatology*, *33*(1), 121–131. https://doi.org/10.1002/joc.3413

Abatzoglou, J. T., & Williams, A. P. (2016). Impact of anthropogenic climate change on wildfire across western US forests. *Proceedings of the National Academy of Sciences*, *113*(42), 11770–11775. https://doi.org/10.1073/pnas.1607171113

Abatzoglou, J. T., Rupp, D. E., O'Neill, L. W., & Sadegh, M. (2021a). Compound extremes drive the western Oregon wildfires of September 2020. *Geophysical Research Letters*, *48*(8), e2021GL092520. https://doi.org/10.1029/2021GL092520

Abatzoglou, J. T., Hatchett, B. J., Fox-Hughes, P., Gershunov, A., & Nauslar, N. J. (2021b). Global climatology of synoptically-forced downslope winds. *International Journal of Climatology*, *41*(1), 31–50. https://doi.org/10.1002/joc.6607

Abatzoglou, J.T., Smith, C.M., Swain, D. L, Ptak, T., & Kolden, C.A. (2020) Population exposure to pre-emptive de-energization aimed at averting wildfires in Northern California. *Environmental Research Letters*, 15(9):94046. https://doi.org/10.1088/1748-9326/aba135

Aguilera, R., Corringham, T., Gershunov, A., & Benmarhnia, T. (2021). Wildfire smoke impacts respiratory health more than fine particles from other sources: observational evidence from Southern California. *Nature communications*, 12(1), 1-8. https://doi.org/10.1038/s41467-021-21708-0

Bellprat, O., Guemas, V., Doblas-Reyes, F., & Donat, M. G. (2019). Towards reliable extreme weather and climate event attribution. *Nature Communications*, *10*(1), 1732. https://doi.org/10.1038/s41467-019-09729-2

Berg, A., & Sheffield, J. (2019). Evapotranspiration Partitioning in CMIP5 Models: Uncertainties and Future Projections. *Journal of Climate*, *32*(10), 2653–2671. https://doi.org/10.1175/JCLI-D-18-0583.1

Bowman, D.M., Kolden, C.A., Abatzoglou, J.T., Johnston, F.H., van der Werf, G.R. and Flannigan, M., 2020. Vegetation fires in the Anthropocene. *Nature Reviews Earth & Environment*, *1*(10), 500-515. https://doi.org/10.1038/s43017-020-0085-3

Chen, B., Jin, Y., Scaduto, E., Moritz, M. A., Goulden, M. L., & Randerson, J. T. (2021a). Climate, fuel, and land use shaped the spatial pattern of wildfire in California's Sierra Nevada. *Journal of Geophysical Research: Biogeosciences*, *126*(2), e2020JG005786. https://doi.org/10.1029/2020JG005786

Donlon, C. J., Martin, M., Stark, J., Roberts-Jones, J., Fiedler, E., & Wimmer, W. (2012). The Operational Sea Surface Temperature and Sea Ice Analysis (OSTIA) system. *Remote Sensing of Environment*, *116*, 140–158. https://doi.org/10.1016/j.rse.2010.10.017

Edinger, J. G. (1964). *Surface Wind Patterns in the Los Angeles Basin During "Santa Ana" Conditions*. University of California, Los Angeles, pp. 100.

Fan, Y., Miguez-Macho, G., Jobbágy, E. G., Jackson, R. B., & Otero-Casal, C. (2017). Hydrologic regulation of plant rooting depth. *Proceedings of the National Academy of Sciences*, *114*(40), 10572–10577. https://doi.org/10.1073/pnas.1712381114

Fosberg, M.A. 1978. Weather in wildland fire management: the fire weather index. In *Proceedings of the Conference on Sierra Nevada Meteorology, Lake Tahoe, California*. Boston.

Goss, M., Swain, D. L., Abatzoglou, J. T., Sarhadi, A., Kolden, C. A., Williams, A. P., & Diffenbaugh, N. S. (2020). Climate change is increasing the likelihood of extreme autumn wildfire conditions across California. *Environmental Research Letters*, *15*(9), 094016. https://doi.org/10.1088/1748-9326/ab83a7

Guillod, B. P., Jones, R. G., Bowery, A., Haustein, K., Massey, N. R., Mitchell, D. M., Otto, F. E. L., Sparrow, S. N., Uhe, P., Wallom, D. C. H., Wilson, S., & Allen, M. R. (2017). weather@home 2: Validation of an improved global–regional climate modelling system. *Geoscientific Model Development*, *10*(5), 1849–1872. https://doi.org/10.5194/gmd-10-1849-2017

Guzman-Morales, J., & Gershunov, A. (2019). Climate Change Suppresses Santa Ana Winds of Southern California and Sharpens Their Seasonality. *Geophysical Research Letters*, *46*(5), 2772–2780. https://doi.org/10.1029/2018GL080261

Hawkins, L. R., Rupp, D. E., McNeall, D. J., Li, S., Betts, R. A., Mote, P. W., Sparrow, S. N., & Wallom, D. C. H. (2019). Parametric sensitivity of vegetation dynamics in the TRIFFID model and the associated uncertainty in projected climate change impacts on western U.S. Forests. *Journal of Advances in Modeling Earth Systems*, *11*(8), 2787–2813. https://doi.org/10.1029/2018MS001577

Hersbach, H., Bell, B., Berrisford, P., Hirahara, S., Horányi, A., Muñoz-Sabater, J., Nicolas, J., Peubey, C., Radu, R., Schepers, D., Simmons, A., Soci, C., Abdalla, S., Abellan, X., Balsamo, G., Bechtold, P., Biavati, G., Bidlot, J., Bonavita, M., … Thépaut, J.-N. (2020). The ERA5 global reanalysis. *Quarterly Journal of the Royal Meteorological Society*, *146*(730), 1999–2049. https://doi.org/10.1002/qj.3803

Hughes, M., Hall, A., & Kim, J. (2011). Human-induced changes in wind, temperature and relative humidity during Santa Ana events. *Climatic Change*, *109*(1), 119–132. https://doi.org/10.1007/s10584-011-0300-9

Jin, Y., Goulden, M. L., Faivre, N., Veraverbeke, S., Sun, F., Hall, A., Hand, M. S., Hook, S., & Randerson, J. T. (2015). Identification of two distinct fire regimes in Southern California: Implications for economic impact and future change. *Environmental Research Letters*, *10*(9), 094005. https://doi.org/10.1088/1748-9326/10/9/094005

Keeley, J. E., & Syphard, A. D. (2019). Twenty-first century California, USA, wildfires: Fuel-dominated vs. wind-dominated fires. *Fire Ecology*, *15*(1), 24. https://doi.org/10.1186/s42408-019-0041-0

Kirchmeier-Young, M. C., Gillett, N. P., Zwiers, F. W., Cannon, A. J., & Anslow, F. S. (2019). Attribution of the influence of human-induced climate change on an extreme fire season. *Earth's Future*, *7*(1), 2–10. https://doi.org/10.1029/2018EF001050

Kolden, C. A., & Abatzoglou, J. T. (2018). Spatial distribution of wildfires ignited under katabatic versus non-katabatic winds in Mediterranean Southern California USA. *Fire*, *1*(2), 19. https://doi.org/10.3390/fire1020019

Kolden, C. A., & Henson, C. (2019). A socio-ecological approach to mitigating wildfire vulnerability in the wildland urban interface: a case study from the 2017 Thomas fire. *Fire*, *2*(1), 9. https://doi.org/10.3390/fire2010009

Lewis, S. C., Blake, S. A., Trewin, B., Black, M. T., Dowdy, A. J., Perkins-Kirkpatrick, S. E., ... & Sharples, J. J. (2020). Deconstructing factors contributing to the 2018 fire weather in Queensland, Australia. [in "Explaining Extremes of 2018 from a Climate Perspective"]. *Bull. Am. Meteorol. Soc.*, *101*, S115-S121. https://doi.org/10.1175/BAMS-D-19-0144.1

Luković, J., Chiang, J. C. H., Blagojević, D., & Sekulić, A. (2021). A later onset of the rainy season in California. *Geophysical Research Letters*, *48*(4), e2020GL090350. https://doi.org/10.1029/2020GL090350

McEvoy, D. J., Pierce, D. W., Kalansky, J. F., Cayan, D. R., & Abatzoglou, J. T. (2020). Projected Changes in Reference Evapotranspiration in California and Nevada: Implications for Drought and Wildland Fire Danger. *Earth's Future*, *8*(11), e2020EF001736. https://doi.org/10.1029/2020EF001736

Miller, N. L., & Schlegel, N. J. (2006). Climate change projected fire weather sensitivity: California Santa Ana wind occurrence. *Geophysical Research Letters*, *33*(15). https://doi.org/10.1029/2006GL025808

Moritz, M. A., Batllori, E., Bradstock, R. A., Gill, A. M., Handmer, J., Hessburg, P. F., ... & Syphard, A. D. (2014). Learning to coexist with wildfire. *Nature*, *515*(7525), 58-66. https://doi.org/10.1038/nature13946

Mote, P. W., Allen, M. R., Jones, R. G., Li, S., Mera, R., Rupp, D. E., Salahuddin, A., & Vickers, D. (2016). Superensemble regional climate modeling for the western United States. *Bulletin of the American Meteorological Society*, *97*(2), 203–215. https://doi.org/10.1175/BAMS-D-14-00090.1

Nauslar, N. J., Abatzoglou, J. T., & Marsh, P. T. (2018). The 2017 North Bay and Southern California Fires: A Case Study. *Fire*, *1*(1), 18. https://doi.org/10.3390/fire1010018

National Academies of Sciences, E. (2016). *Attribution of Extreme Weather Events in the Context of Climate Change*. https://doi.org/10.17226/21852

Rogers, B. M., Balch, J. K., Goetz, S. J., Lehmann, C. E. R., & Turetsky, M. (2020). Focus on changing fire regimes: Interactions with climate, ecosystems, and society. *Environmental Research Letters*, *15*(3), 030201. https://doi.org/10.1088/1748-9326/ab6d3a

Schaller, N., Otto, F. E. L., van Oldenborgh, G. J., Massey, N. R., Sparrow, S., & Allen, M. R. (2014). The heavy precipitation event of May-June 2013 in the Upper Danube and Elbe Basins. [in "Explaining extremes of 2013 from a climate perspective"], *Bulletin American Meteorological Society*, *95*(9), S69-S72.

Smith, C., Hatchett, B. J., & Kaplan, M. (2018). A surface observation based climatology of Diablo-Like winds in California's wine country and western Sierra Nevada. *Fire*, *1*(2), 25. https://doi.org/10.3390/fire1020025

Srock, A. F., Charney, J. J., Potter, B. E., & Goodrick, S. L. (2018). The Hot-Dry-Windy Index: A new fire weather index. *Atmosphere*, *9*(7), 279. https://doi.org/10.3390/atmos9070279

Stavros, E. N., Abatzoglou, J., Larkin, N. K., McKenzie, D., Steel, E. A., Stavros, E. N., Abatzoglou, J., Larkin, N. K., McKenzie, D., & Steel, E. A. (2014). Climate and very large wildland fires in the contiguous western USA. *International Journal of Wildland Fire*, *23*(7), 899–914. https://doi.org/10.1071/WF13169

Swain, D. L., Langenbrunner, B., Neelin, J. D. & Hall, A. (2018) Increasing precipitation volatility in twenty-first-century California. *Nature Climate Change, 8*, 427. https://doi.org/10.1038/s41558-018-0140-y

Swain, D. L. (2021). A shorter, sharper rainy season amplifies California wildfire risk. *Geophysical Research Letters*, *48*(5), e2021GL092843. https://doi.org/10.1029/2021GL092843

Tan, X., Chen, S., & Gan, T. Y. (2018). Multi-model extreme event attribution of the weather conducive to the 2016 Fort McMurray wildfire. *Agricultural and Forest Meteorology*, *260–261*, 109–117. https://doi.org/10.1016/j.agrformet.2018.06.010

*Twenty-first century California, USA, wildfires: Fuel-dominated vs. Wind-dominated fires | Fire Ecology | Full Text*. (n.d.). Retrieved May 1, 2021, from https://fireecology.springeropen.com/articles/10.1186/s42408-019-0041-0

Uhe, P., Otto, F. E. L., Haustein, K., Oldenborgh, G. J. van, King, A. D., Wallom, D. C. H., Allen, M. R., & Cullen, H. (2016). Comparison of methods: Attributing the 2014 record

European temperatures to human influences. *Geophysical Research Letters*, *43*(16), 8685–8693. https://doi.org/10.1002/2016GL069568

Uhe, P., Mitchell, D., Bates, P. D., Allen, M. R., Betts, R. A., Huntingford, C., King, A. D., Sanderson, B. M., & Shiogama, H. (2021). Method uncertainty Is essential for reliable confidence statements of precipitation projections. *Journal of Climate*, *34*(3), 1227–1240. https://doi.org/10.1175/JCLI-D-20-0289.1

van Oldenborgh, G. J., Krikken, F., Lewis, S., Leach, N. J., Lehner, F., Saunders, K. R., van Weele, M., Haustein, K., Li, S., Wallom, D., Sparrow, S., Arrighi, J., Singh, R. K., van Aalst, M. K., Philip, S. Y., Vautard, R., & Otto, F. E. L. (2021). Attribution of the Australian bushfire risk to anthropogenic climate change. *Natural Hazards and Earth System Sciences*, *21*(3), 941–960. https://doi.org/10.5194/nhess-21-941-2021

Van Wagner et al., (1987). Development and Structure of the Canadian Forest Fire Weather Index System. *European Environment Agency*. (n.d.). [Methodology Reference]. Retrieved May 1, 2021, from https://www.eea.europa.eu/data-and-maps/indicators/forest-fire-danger-3/camia-et-al.-2008-past

Wang, M., Ullrich, P., & Millstein, D. (2020). Future projections of wind patterns in California with the variable-resolution CESM: A clustering analysis approach. *Climate Dynamics*, *54*(3), 2511–2531. https://doi.org/10.1007/s00382-020-05125-5

Williams, A. P., Abatzoglou, J. T., Gershunov, A., Guzman-Morales, J., Bishop, D. A., Balch, J. K., & Lettenmaier, D. P. (2019). Observed impacts of anthropogenic climate change on wildfire in California. *Earth's Future*, *7*(8), 892–910. https://doi.org/10.1029/2019EF001210

Yue, X., Mickley, L. J., & Logan, J. A. (2014). Projection of wildfire activity in southern California in the mid-twenty-first century. *Climate Dynamics*, *43*(7), 1973–1991. https://doi.org/10.1007/s00382-013-2022-3

Geophysical Research Letters

Supporting Information for

# Anthropogenic influence on recent severe autumn fire weather in the west coast of the United States

Linnia R. Hawkins[1], John T. Abatzoglou[2], Sihan Li[3,4], David E. Rupp[5]

[1]Forest Ecosystems & Society Department, Oregon State University, Corvallis, OR, USA, [2]Management of Complex Systems Department, University of California Merced, Merced, CA, USA, [3]Environmental Change Institute, School of Geography and the Environment, University of Oxford, Oxford, UK, [4]Oxford e-Research Centre, University of Oxford, Oxford, UK, [5]Oregon Climate Change Research Institute, College of Earth, Ocean, and Atmospheric Science, Oregon State University, Corvallis, OR, USA

**Contents of this file**



**Introduction**

This supporting information contains additional technical details of the methodologies used in sections S1-S3 as well as figures S1-S8 and tables S1-S5.

**Section S1. Experimental design**

The analyses of this study are based on two sets of attribution experiments, one using modelled outputs to calculate fire weather indices (*fire weather experiment*) and the other using modelled outputs to perform the wind analysis (*wind experiment*). Each set of experiments consisted of an ensemble of simulations representing modern-era climate conditions, referred to as actualClim, and an ensemble of simulations representing pre-industrial climate (i.e. without anthropogenic influence), referred to as naturalClim. The actualClim and naturalClim ensembles covered the same time period, with the actualClim ensembles using observed concentrations of greenhouse gases and observation-based SSTs and sea ice fractions (SIC) from the Operational Sea Surface Temperature and Sea Ice Analysis (OSTIA; Donlon et al. 2012). Whereas the naturalClim ensembles used pre-industrial level greenhouse gases and pre-industrial SST and SIC, constructed by removing anthropogenic signals from the OSTIA observed values. Thirteen estimates of anthropogenic SST (deltaSST) warming patterns were used, 12 from CMIP5 models, and 1 from the multi-model mean constructed from these 12 models. The deltaSST calculations are detailed in Schaller et al. (2014).

The *fire weather experiment* covered Sep2016-Dec2018, with Sep through Nov 2016 excluded from the analysis due to the lack of antecedent information needed for calculating fuel moisture in autumn 2016. The *wind experiment* covered Sep2017-Dec2018. Model outputs consisted of daily values (precipitation) or instantaneous values (10-m wind speed, 2-m temperature, 2-m relative humidity from the *fire weather experiment* and wind velocity, temperature, geopotential height at various pressure levels from the *wind experiment*) at 21Z (1300 LST) corresponding to the approximate times used in calculating daily fire danger rating systems.

**S2. Comparison of 700-hPa wind climatology from HadAM-RM3p and reanalysis**

We compared wind climatology between the HadAM-RM3p ensemble and ECMWF ReAnalysis 5 (ERA5; Hersbach et al., 2020) because ERA5 has a similar horizontal resolution (30 km) to HadRM3p (~25 km) and is the state-of-the-art reanalysis. We used the years 1979-2019 from ERA5. From the HadAM-RM3p ensemble, the distribution of winds represents internal atmospheric variability in the year 2018 only, so it is expected that the distribution is narrower than it would be if the SSTs from 1979 to 2019 were used as the boundary conditions to HadAM-RM3p.

From the *wind experiment* with HadAM-RM3p, winds on several pressure levels were saved daily at 21 Z for 402 initial condition ensemble members; the sample size = 12,060 wind fields per pressure level per month (402 ensemble members × 30 days per month).

Figures S1-S3 show frequency distributions of wind speed and direction, as wind roses, for the months of autumn (September, October, and November) at 700-hPa for example locations in Regions ORa, CAa, and CAd, respectively. The precise locations are shown in Fig. 4d and identified by the solid black circle in each region.

**S3. Identification and examination of offshore downslope winds in the HadAM-RM3p ensemble**

In the HadAM-RM3p ensemble, we identified conditions suitable for offshore, downslope winds (ODWs) in six regions from northern Oregon to southern California, with each region consisting of 16 model grid cells in a 4x4 matrix (See region locations in Fig. 4d). We adapted the method of Abatzoglou et al. (2021b) to identify instances of such conditions based on the cross-barrier 700-hPa horizontal wind speed $u \geq 13$ m s-1 and the 700-hPa vertical wind speed $\omega \geq 0.6$ Pa s-1 at 21 Z in a grid cell. Within a region, the $u$ and $\omega$ criteria did not have to be met in the same grid cell for the instance to qualify. The cross-barrier wind direction varied by region to accommodate the primary direction of offshore flow and orientation of orography: 90°, 60°, and 45° for the Cascades, Sierras, and Transverse Ranges, respectively. We added the criterion of near-surface $RH \leq 30\%$ (e.g., Edinger et al., 1964; Smith et al., 2018) to further constrain focus on wind events that yield elevated fire weather potential.

We further determined if the climate model would simulate lower troposphere and near-surface conditions associated with ODWs as, or more, extreme as those during several of the recent large autumn wildfires in California and Oregon. We used the same general method for identifying ODWs described above but considered extreme ODW using more stringent criteria: Cross-barrier 700-hPa wind speed > 18 m $s^{-1}$, 700-hPa $\omega > 1.5$ Pa $s^{-1}$, and near-surface $RH < 20\%$.

Simulated ODW frequency in autumn varied regionally from < 1 day per autumn in the Oregon Cascades (ORa and ORb) to nearly 3 days per autumn in Transverse Ranges (CAd) (Table S1). Along the Sierra Nevada, frequencies decreased from north to south, consistent with diagnostics from ERA5 (Abatzolgou et al., 2021b). However, frequencies were sensitive to the selected cross-barrier wind direction and the exact locations of the analysis regions, so precise comparisons between regions should not be made based on these results.

The HadAM-RM3p actualClim ensemble contained instances of extreme ODWs in all regions in autumn (Table S1). Extreme ODWs were rarest in the Oregon Cascades (0.09 instances per autumn on average), and most frequent in Transverse Ranges (0.96 instances per autumn).

Figures S4-S6 show latitudinal profiles of wind velocity and air temperature in the lower troposphere during examples of extreme ODWs in Regions ORa, CAa, and CAd, respectively. The figures show one snapshot of extreme ODWs for each region from three unique model simulations to illustrate the signature of ODWs. In the Oregon Cascades example (ORa; Fig. S4), the ODW criteria were met on three consecutive days at 21 Z and the maximum 700-hPa cross-barrier wind speed and $\omega$ were 21.0 m $s^{-1}$ and 2.2 Pa $s^{-1}$, respectively while the minimum surface *RH* was 6.1%. In the Sierras example (CAa; Fig. S5), the criteria were met on two consecutive days at 21 Z and the maximum 700-hPa cross-barrier wind speed and $\omega$ were 34.6 m $s^{-1}$ and 5.3 Pa $s^{-1}$, respectively, while the minimum surface *RH* was 9.9%. Fig. S5 also shows the characteristic temperature inversion that can develop during these events (e.g., Abatzoglou et al. 2021b) persisting into the afternoon. For the Transverse Ranges example (CAd; Fig. S6), the criteria were met on two consecutive days at 21 Z and the maximum 700-hPa cross-barrier wind speed and $\omega$ were 29.8 m $s^{-1}$ and 5.1 Pa $s^{-1}$, respectively while the minimum surface *RH* was 9.2%.

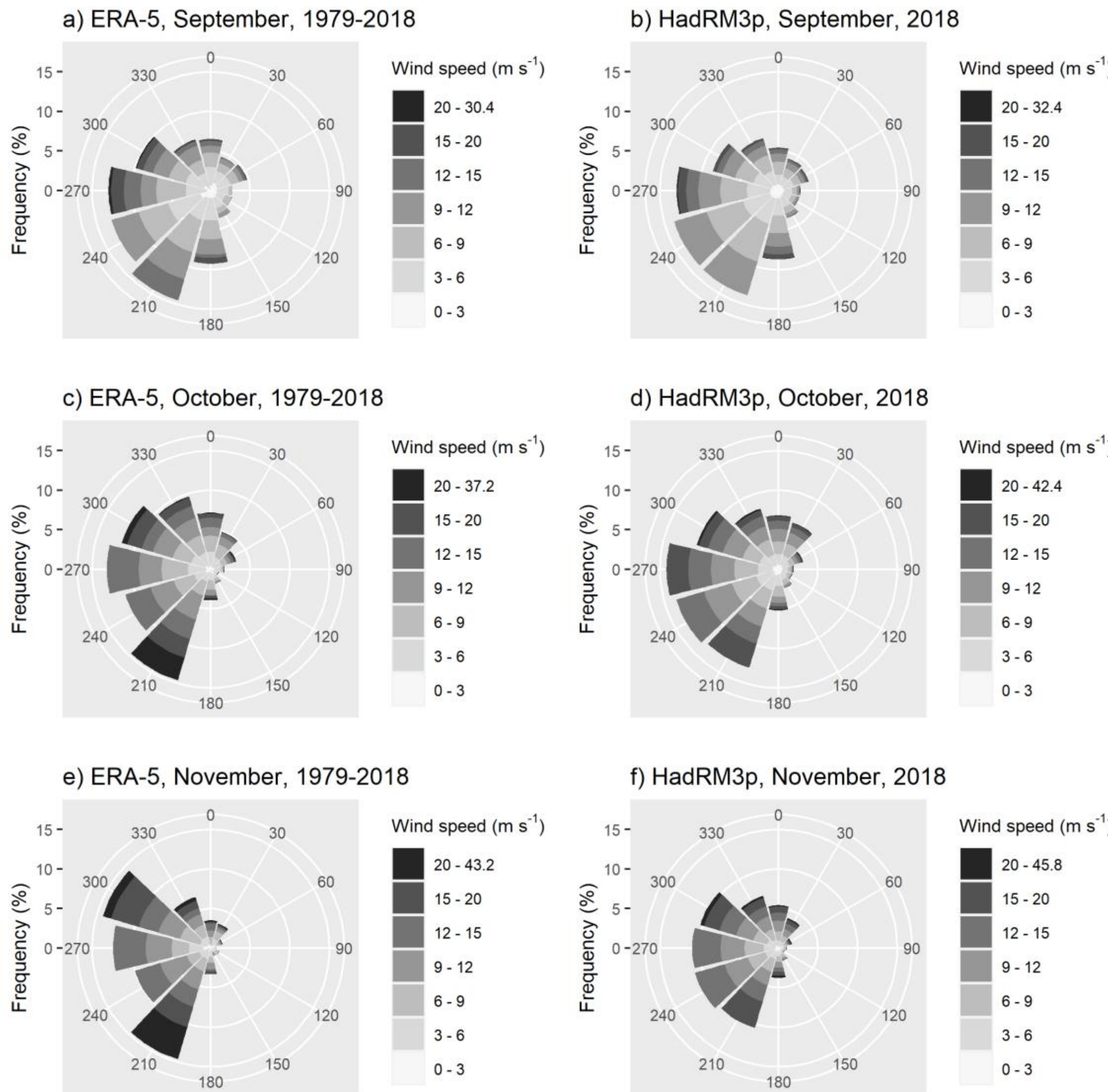


**Figure S1.** Frequency distribution of 700-hPa wind speed and wind direction at 21 Z for a location in Region ORa in **(a, b)** September, **(c, d)** October, and **(e, f)** November from **(a, c, e)** ERA5, 1979-2019 (-122.25°E, 44.75°N) and **(b, d, f)** and the HadAM-RM3p 402-member ensemble (-122.3733°E, 44.8175°N).

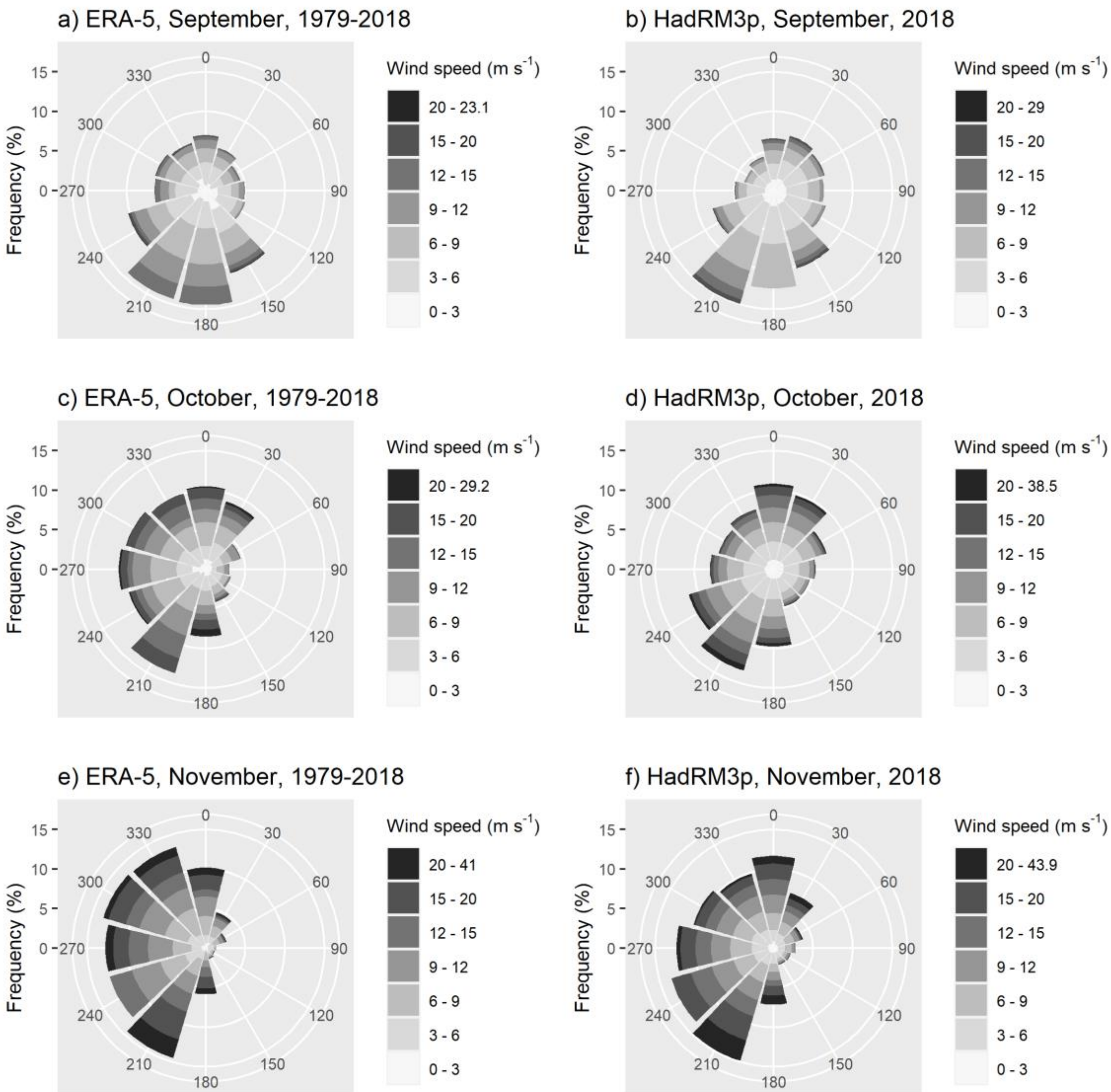


**Figure S2.** Fame as Figure S2 but for a location in Region CAa from ERA5 (-121.75°E, 40.00°N) and HadAM-RM3p (-121.7413°E, 39.9799°N).

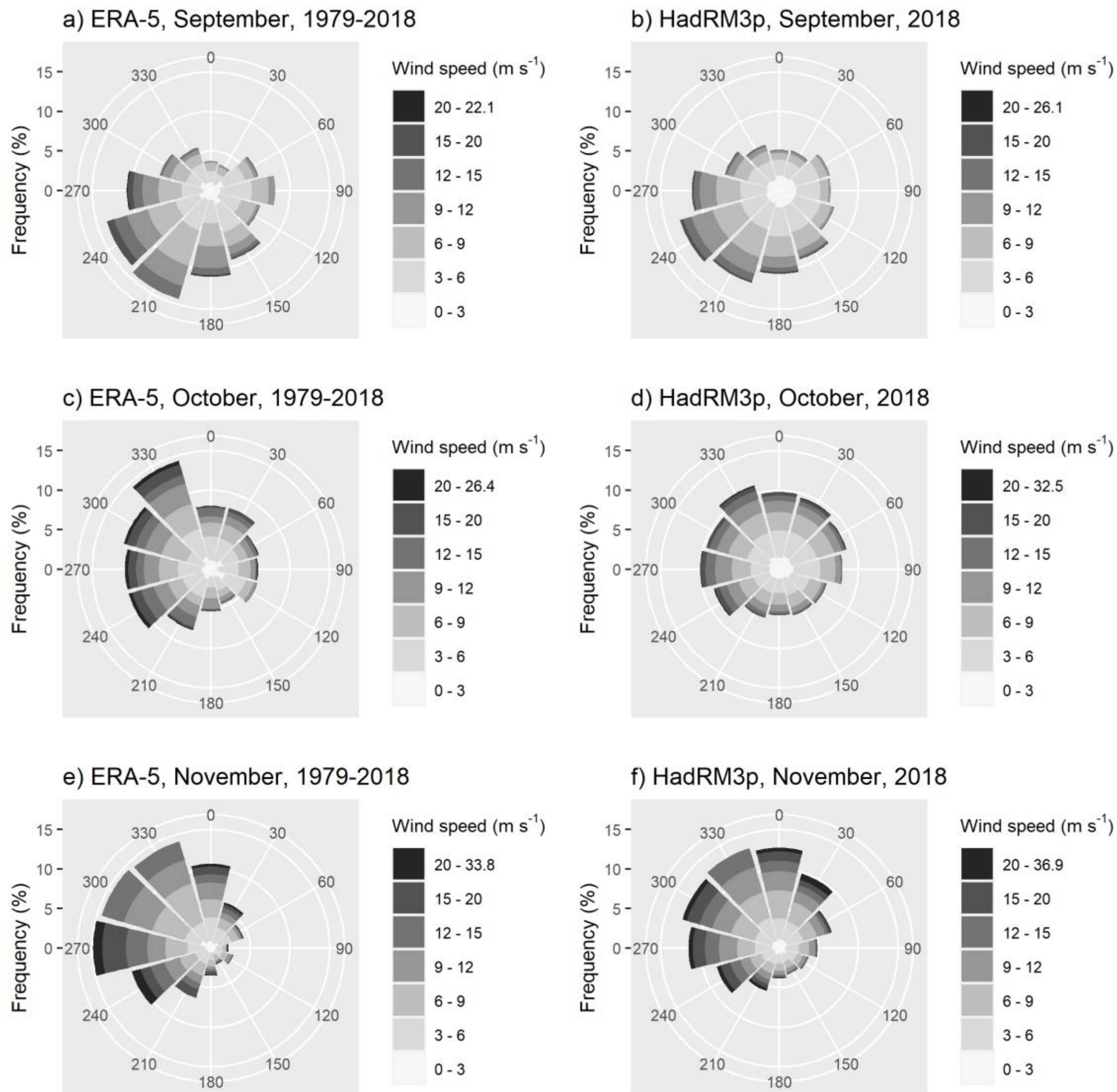


**Figure S3.** Same as Figure S2 but for a location in Region CAd from ERA5 (-118.50°E, 34.50°N) and HadAM-RM3p (-118.5516°E, 34.4359°N).

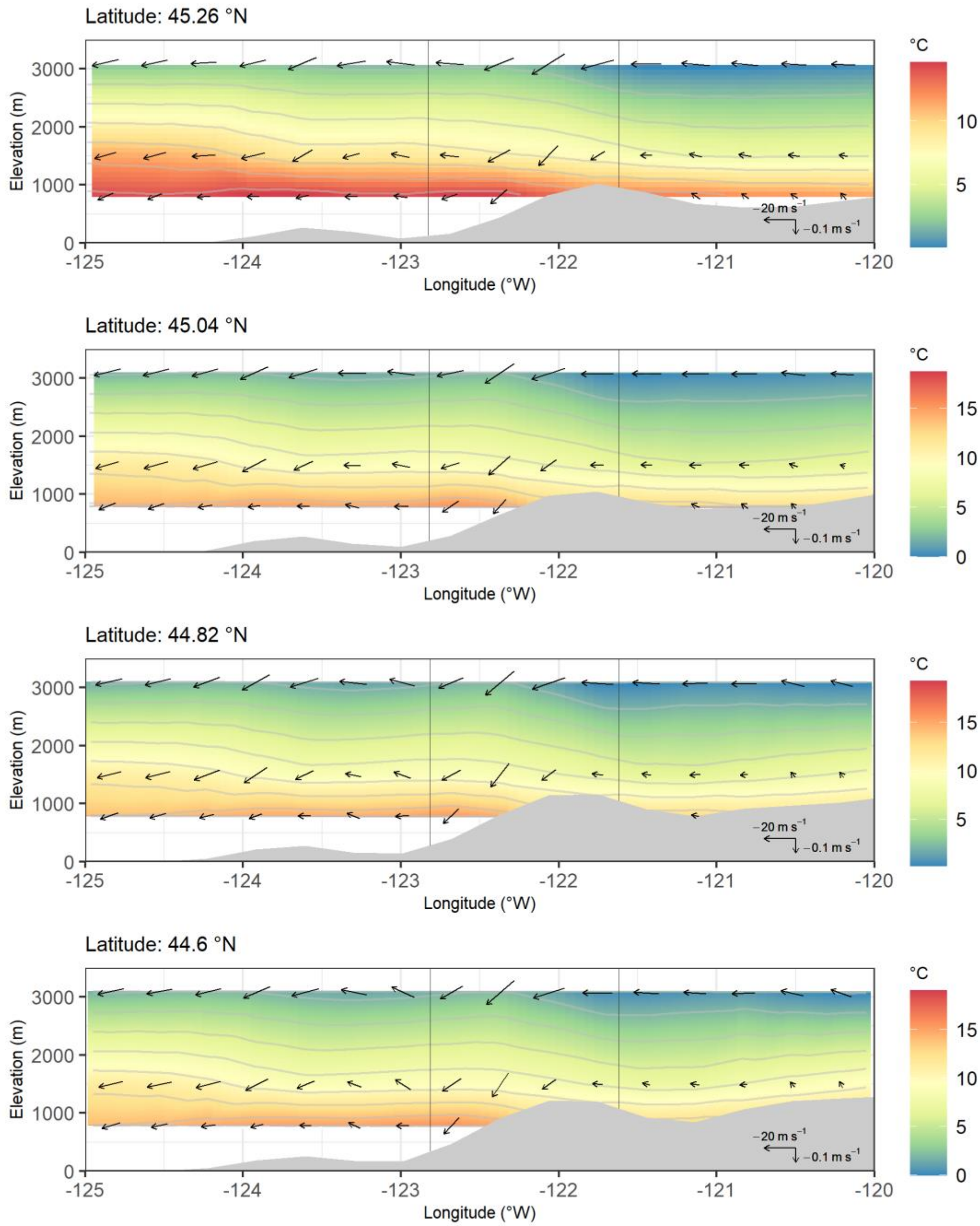


**Figure S4.** Example of simulated temperature and winds along 4 latitudinal transects at 21 Z meeting criteria for extreme downslope wind conditions on an autumn day in Region ORa (see Figure 4d). Gray shading shows land. The two vertical gray lines mark the east and west boundaries of the 4 x 4 grid used when determining extreme downslope wind conditions. Temperature was bilinearly interpolated from points at the 925, 850 and 700-hPa pressure levels. Latitude designations are approximate for each panel because the regional model grid is not oriented along lines of global latitude and longitude.

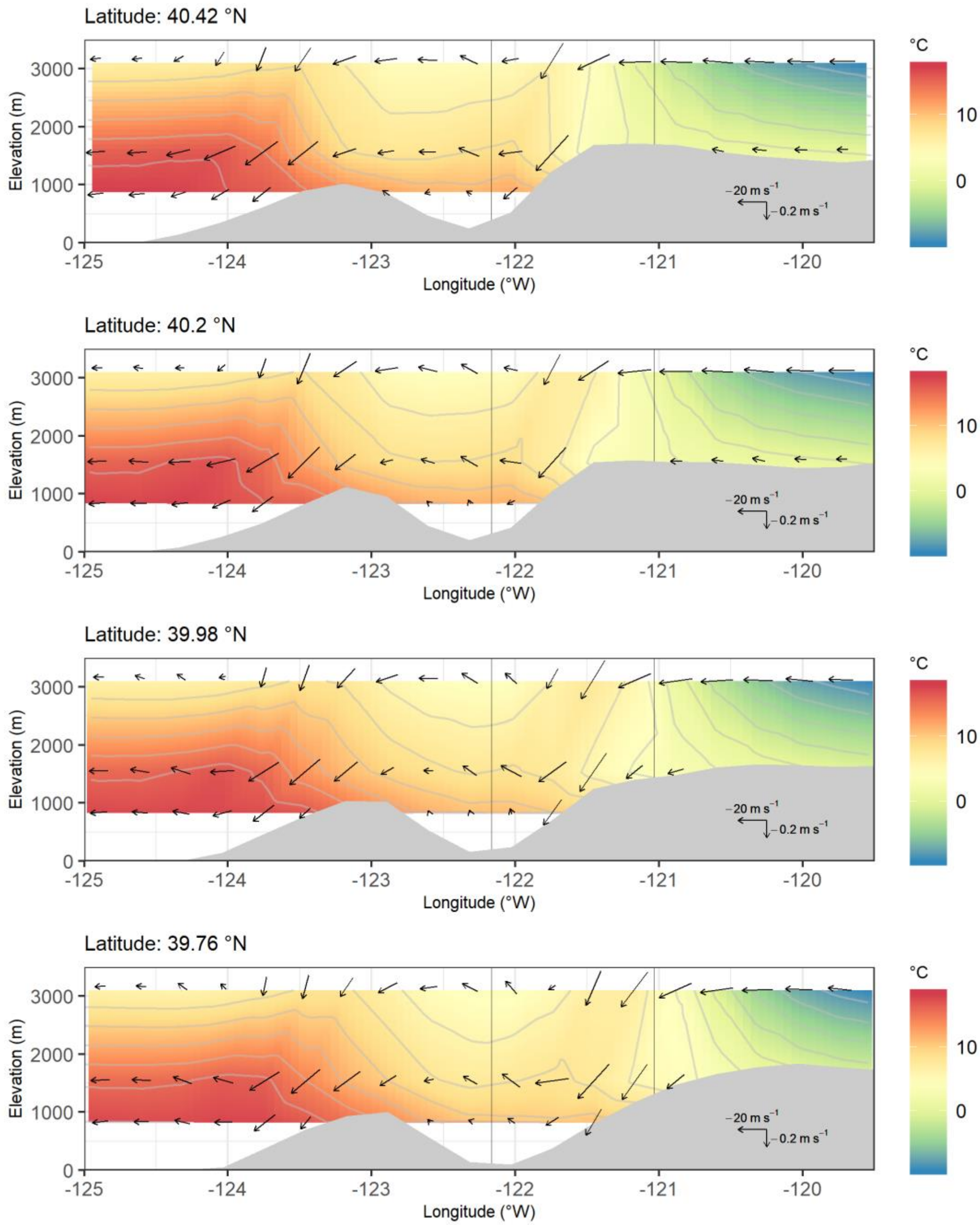


**Figure S5.** Same as Fig. S4 but for Region CAa.

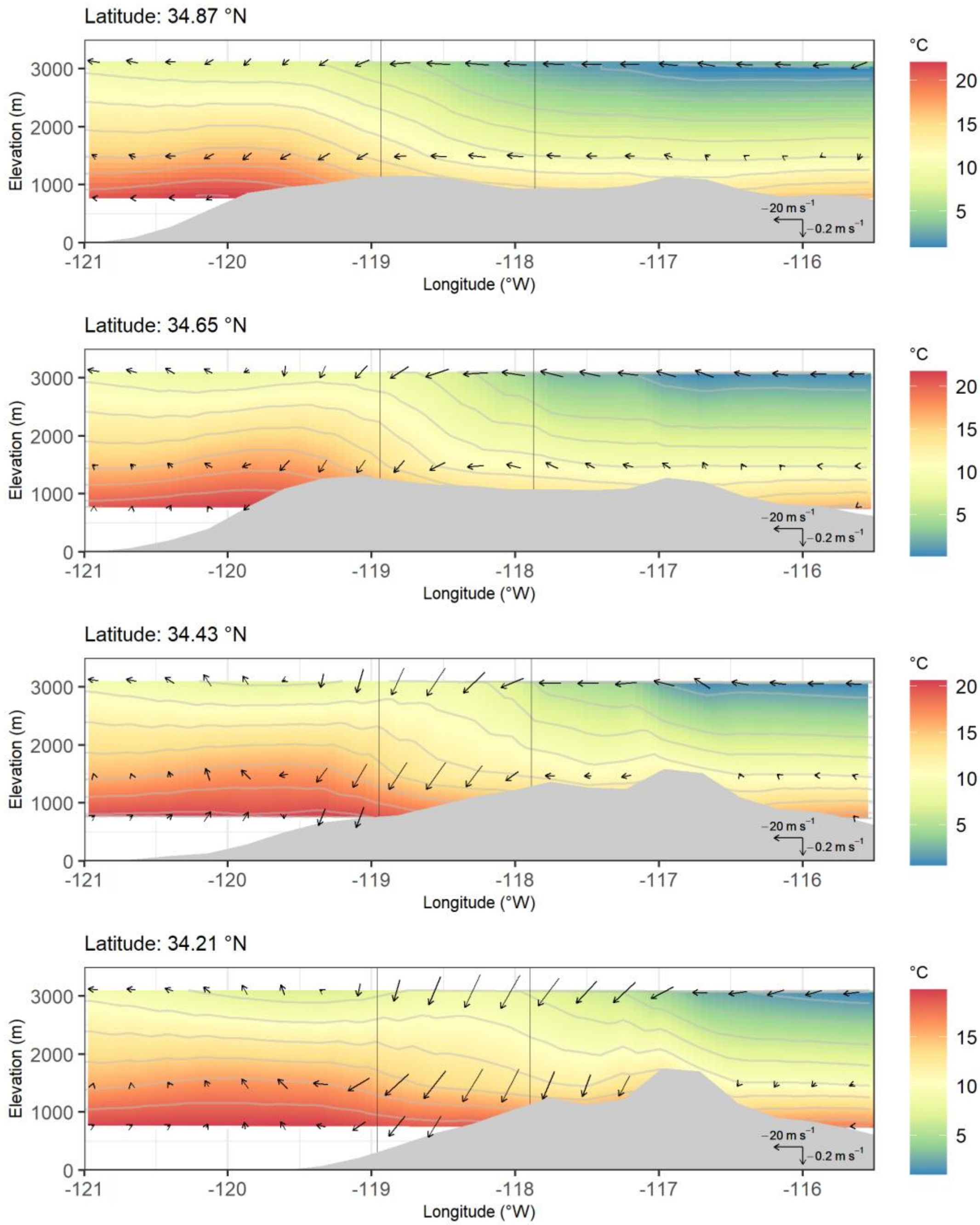


**Figure S6.** Same as Fig. S4 but for Region CAd.

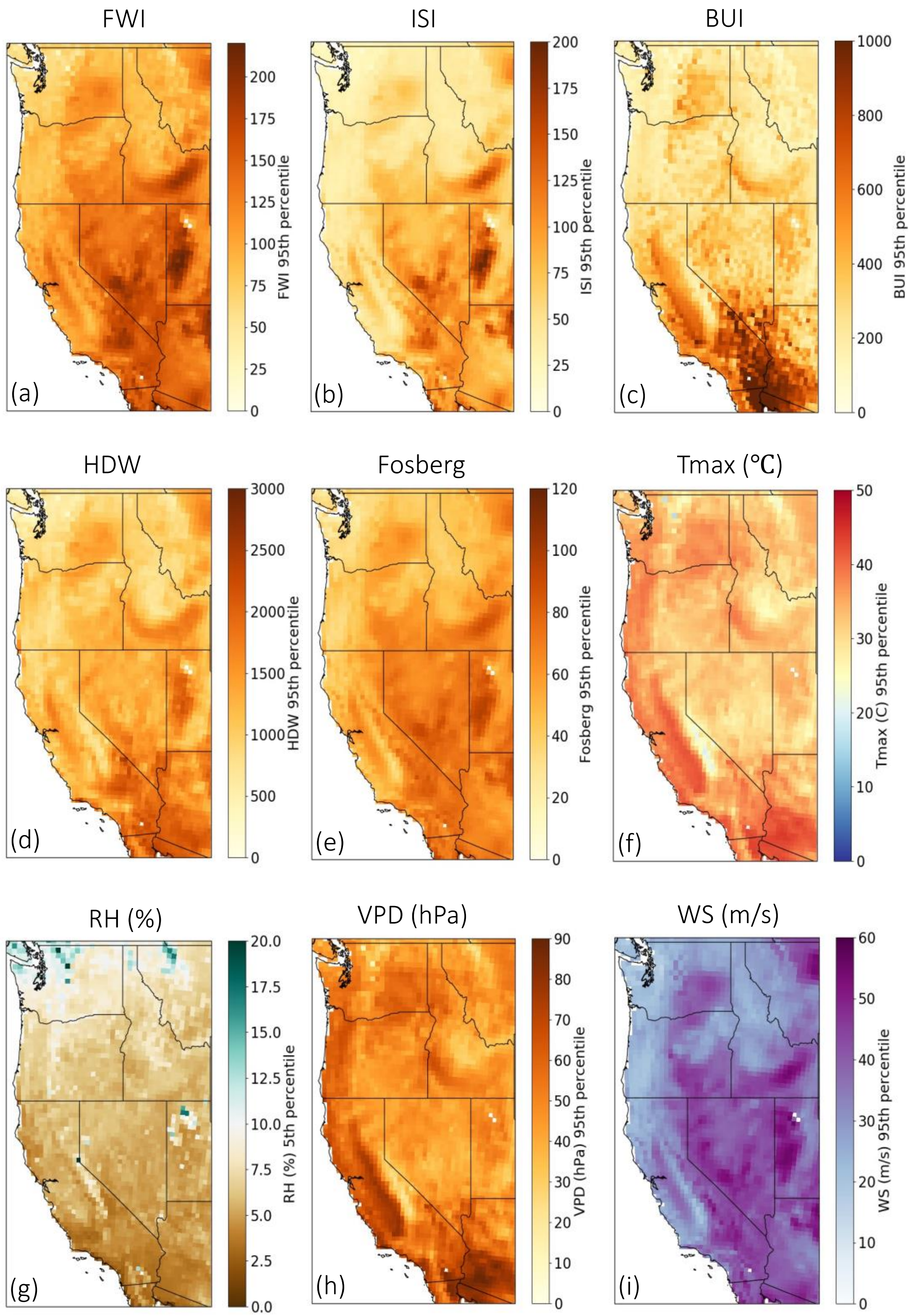


**Figure S7.** ActualClim ensemble 95th percentile of autumn (SON) maximum FWI and the concurrent fire weather indices and meteorological conditions by grid cell. For RH, the 5th percentile is shown.

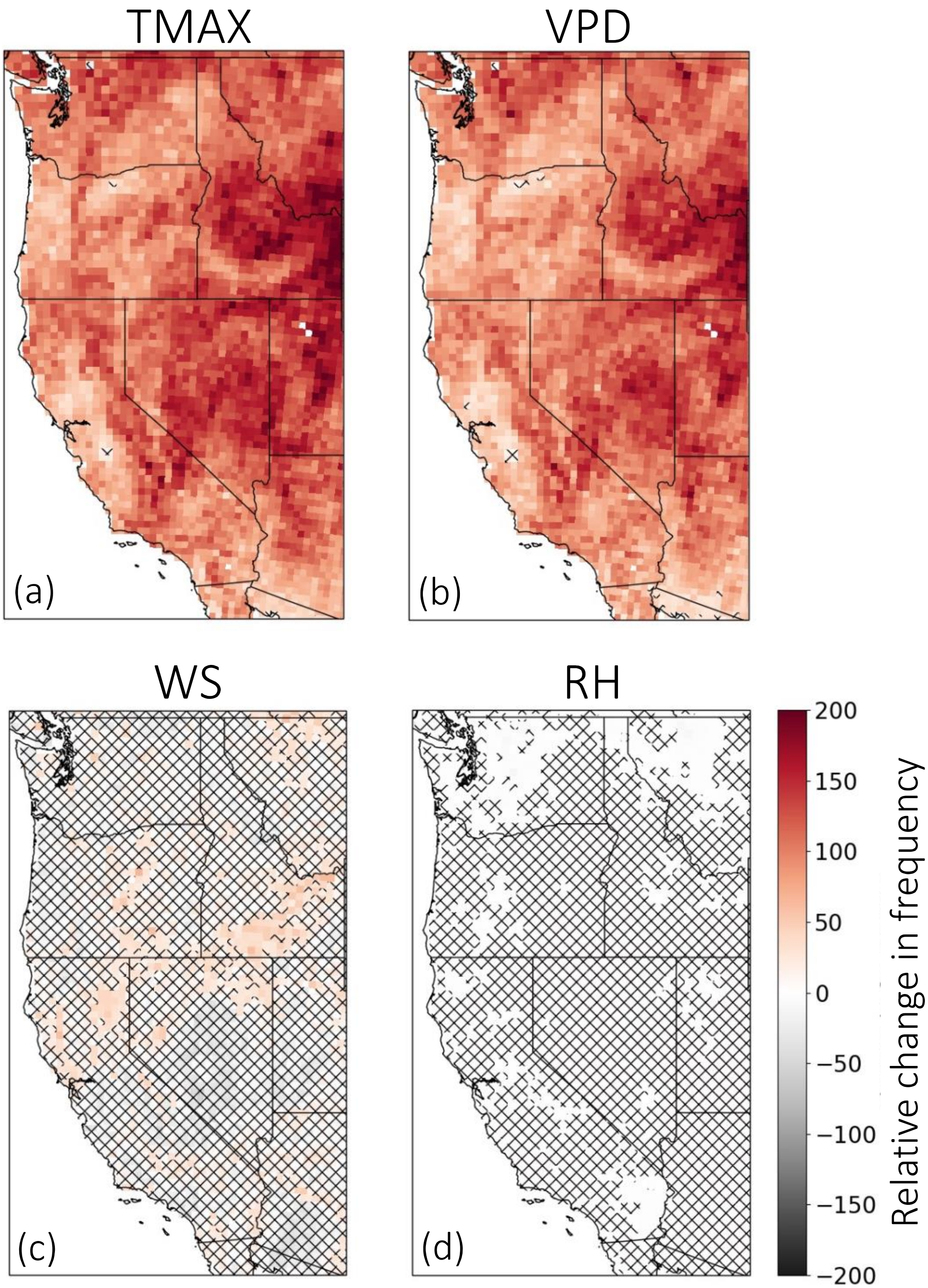


**Figure S8.** Relative change in frequency of extreme high (>95th percentile) autumn (SON) 21Z temperature (a) vapor pressure deficit (c) wind speed (d) and extreme low (<5th percentile) 21Z relative humidity (b) concurrent with the $FWI_{max}$ between naturalClim and actualClim simulations.

**Table S1.** Summary of the simulated change in frequency (%) of fire weather indices and meteorological variables between actualClim and naturalClim ensembles, averaged over western US domain (approximately 35.2N–48.8N, 124W–109W).

| Variable | Percent of domain with significant increases | Regional mean change in frequency |
|---|---|---|
| FWI | 65% | +39% |
| ISI | 52% | +27% |
| BUI | 86% | +60% |
| HDW | 99% | +105% |
| FFWI | 20% | +9% |
| TA | 99% | +117% |
| RH | 18% | 0% |
| VPD | 99% | +105% |
| WS | 11% | +4% |

**Table S2.** Summary of the differences in meteorological variables in simulations where fire weather indices above the respective $95^{th}$ percentile in actualClim and naturalClim ensembles, averaged over western US domain (approximately 35.2N–48.8N, 124W–109W).

| Variable | Temperature (C) | Relative Humidity (%) | VPD (hPa) | Wind Speed (m/s) |
|---|---|---|---|---|
| FWI | 1.15 | 0.10 | 1.52 | -0.17 |
| ISI | 1.13 | 0.01 | 1.51 | -0.08 |
| BUI | 0.97 | 0.11 | 1.21 | 0.25 |
| HDW | 1.11 | -0.04 | 2.16 | -0.07 |
| FFWI | 1.09 | 0.13 | 1.22 | -0.04 |

**Table S3.** Difference (and fractional difference) in frequency between naturalClim and actualClim of Offshore Downslope Winds and Extreme Offshore Downslope Winds at 21 Z in the Autumn Fire Season (September-November).

| Region | Variable | Natural forcings | All forcings | Anthropogenic effect | C.I.[c] |
|---|---|---|---|---|---|
| | | Offshore Downslope Winds | | | |
| ORa | Days per season | 0.72 | 0.66 | -0.06[a] | (-0.16,0.05) |
| | Probability | 0.0080 | 0.0074 | -0.08[b] | (-0.21,0.07) |
| ORb | Days per season | 0.77 | 0.69 | -0.08[a] | (-0.19,0.03) |
| | Probability | 0.0086 | 0.0077 | -0.10[b] | (-0.23,0.04) |
| CAa | Days per season | 2.77 | 2.57 | -0.19[a] | (-0.41,0.01) |
| | Probability | 0.0308 | 0.0286 | -0.07[b] | (-0.14,0.01) |
| CAb | Days per season | 2.65 | 2.46 | -0.19a | (-0.39,0.02) |
| | Probability | 0.0294 | 0.0274 | -0.07[b] | (-0.14,0.01) |
| CAc | Days per season | 1.24 | 1.16 | -0.09[a] | (-0.23,0.06) |
| | Probability | 0.0138 | 0.0129 | -0.07[b] | (-0.18,0.05) |
| CAd | Days per season | 2.88 | 2.67 | **-0.21[a]** | (-0.42,-0.01) |
| | Probability | 0.0320 | 0.0297 | **-0.07[b]** | (-0.14,-0.00) |
| | | Extreme Offshore Downslope Winds | | | |
| ORa | Days per season | 0.09 | 0.09 | 0.00[a] | (-0.03,0.03) |
| | Probability | 0.0010 | 0.0010 | -0.01[b] | (-0.54,0.29) |
| ORb | Days per season | 0.14 | 0.11 | -0.03[a] | (-0.06,0.01) |
| | Probability | 0.0015 | 0.0012 | -0.19[b] | (-0.74,0.08) |
| CAa | Days per season | 0.71 | 0.68 | -0.03[a] | (-0.13,0.07) |
| | Probability | 0.0079 | 0.0076 | -0.04[b] | (-0.21,0.09) |
| CAb | Days per season | 0.80 | 0.65 | **-0.14[a]** | (-0.24,-0.04) |
| | Probability | 0.0089 | 0.0073 | **-0.18[b]** | (-0.40,-0.06) |
| CAc | Days per season | 0.32 | 0.34 | 0.02[a] | (-0.05,0.09) |
| | Probability | 0.0036 | 0.0038 | 0.06[b] | (-0.17,0.22) |
| CAd | Days per season | 0.96 | 0.92 | -0.04[a] | (-0.16,0.07) |
| | Probability | 0.0107 | 0.0102 | -0.05[b] | (-0.19,0.07) |

[a]Difference: actualClim – naturalClim.

[b]Fractional difference: (actualClim – naturalClim) / naturalClim.

[a,b]Bold-faced values have confidence intervals that do not include 0.

[c]95% confidence interval (C.I.)

**Table S4.** Difference (and fractional difference) between naturalClim and actualClim Near-Surface Conditions during Offshore Downslope Winds at 21 Z in the Autumn Fire Season (September-November).

| Region | Variable | Natural Clim | Actual Clim | Anthropogenic effect | C.I.[c] |
|---|---|---|---|---|---|
| ORa | 2-m temperature anomaly (°C) | -0.80 | 0.63 | **1.43**[a] | (0.85,2.01) |
| | 2-m relative humidity (%) | 21.13 | 20.33 | -0.04[b] | (-0.07,0.00) |
| | 2-m vapor pressure deficit (kPa) | 1.560 | 1.698 | **0.09**[b] | (0.03,0.15) |
| | 10-m wind speed (m $s^{-1}$) | 22.79 | 22.61 | -0.01[b] | (-0.03,0.01) |
| ORa | 2-m temperature anomaly (°C) | -0.09 | 0.90 | **0.99**[a] | (0.42,1.54) |
| | 2-m relative humidity (%) | 18.26 | 17.86 | -0.02[b] | (-0.06,0.02) |
| | 2-m vapor pressure deficit (kPa) | 1.903 | 2.016 | **0.06**[b] | (0.00,0.12) |
| | 10-m wind speed (m $s^{-1}$) | 16.29 | 16.40 | 0.01[b] | (-0.02,0.03) |
| CAa | 2-m temperature anomaly (°C) | -1.57 | -0.48 | **1.09**[a] | (0.85,1.33) |
| | 2-m relative humidity (%) | 16.68 | 16.28 | -0.02[b] | (-0.05,0.00) |
| | 2-m vapor pressure deficit (kPa) | 1.872 | 1.963 | **0.05**[b] | (0.01,0.09) |
| | 10-m wind speed (m $s^{-1}$) | 15.85 | 16.26 | 0.03[b] | (0.00,0.05) |
| CAb | 2-m temperature anomaly (°C) | -1.24 | -0.39 | **0.85**[a] | (0.58,1.12) |
| | 2-m relative humidity (%) | 16.59 | 16.47 | -0.01[b] | (-0.03,0.02) |
| | 2-m vapor pressure deficit (kPa) | 2.159 | 2.273 | **0.05**[b] | (0.03,0.08) |
| | 10-m wind speed (m $s^{-1}$) | 21.48 | 21.63 | 0.01[b] | (-0.01,0.03) |
| CAc | 2-m temperature anomaly (°C) | -1.51 | -0.68 | **0.84**[a] | (0.49,1.18) |
| | 2-m relative humidity (%) | 17.48 | 17.19 | -0.02[b] | (-0.05,0.02) |
| | 2-m vapor pressure deficit (kPa) | 1.872 | 1.963 | **0.05**[b] | (0.01,0.09) |
| | 10-m wind speed (m $s^{-1}$) | 16.92 | 16.94 | 0.00[b] | (-0.03,0.04) |
| CAd | 2-m temperature anomaly (°C) | -1.44 | -0.61 | **0.83**[a] | (0.60,1.06) |
| | 2-m relative humidity (%) | 12.25 | 12.23 | 0.00[b] | (-0.03,0.03) |
| | 2-m vapor pressure deficit (kPa) | 2.374 | 2.486 | **0.05**[b] | (0.02,0.07) |
| | 10-m wind speed (m $s^{-1}$) | 29.56 | 29.73 | 0.01[b] | (0.00,0.02) |

[a]Difference: all forcings – natural forcings.

[b]Fractional difference: (all forcings – natural forcings) / natural forcings.

[a],[b]Bold-faced values have confidence intervals that do not include 0.

[c]95% confidence interval (C.I.)

**Table S5.** Difference (or fractional difference) between naturalClim and actualClim Near-Surface Conditions during Extreme Offshore Downslope Winds at 21 Z in the Autumn Fire Season (September-November).

| Region | Variable | Natural Clim | Actual Clim | Anthropogenic effect | C.I.[c] |
|---|---|---|---|---|---|
| ORa | 2-m temperature anomaly (°C) | -3.34 | -0.98 | **2.36**[a] | (0.60,4.03) |
| | 2-m relative humidity (%) | 15.67 | 13.89 | **-0.11**[b] | (-0.18,-0.04) |
| | 2-m vapor pressure deficit (kPa) | 1.384 | 1.731 | **0.25**[b] | (0.08,0.44) |
| | 10-m wind speed (m $s^{-1}$) | 26.32 | 25.22 | -0.04[b] | (-0.08,0.00) |
| ORa | 2-m temperature anomaly (°C) | -1.98 | -0.63 | **1.35**[a] | (-0.18,2.82) |
| | 2-m relative humidity (%) | 14.0 | 13.31 | -0.05[b] | (-0.13,0.03) |
| | 2-m vapor pressure deficit (kPa) | 1.653 | 1.878 | 0.14[b] | (-0.01,0.30) |
| | 10-m wind speed (m $s^{-1}$) | 19.04 | 19.77 | 0.04[b] | (-0.01,0.09) |
| CAa | 2-m temperature anomaly (°C) | -2.26 | -0.87 | **1.39**[a] | (0.98,1.79) |
| | 2-m relative humidity (%) | 12.96 | 13.01 | 0.00[b] | (-0.03,0.04) |
| | 2-m vapor pressure deficit (kPa) | 2.297 | 2.452 | **0.07**[b] | (0.02,0.11) |
| | 10-m wind speed (m $s^{-1}$) | 18.41 | 19.13 | 0.04[b] | (0.00,0.08) |
| CAb | 2-m temperature anomaly (°C) | -1.77 | -1.00 | **0.77**[a] | (0.30,1.25) |
| | 2-m relative humidity (%) | 12.61 | 12.93 | 0.03[b] | (-0.01,0.06) |
| | 2-m vapor pressure deficit (kPa) | 2.194 | 2.223 | 0.01[b] | (-0.03,0.06) |
| | 10-m wind speed (m $s^{-1}$) | 26.37 | 26.93 | 0.02[b] | (0.00,0.05) |
| CAc | 2-m temperature anomaly (°C) | -1.51 | -0.51 | **0.99**[a] | (0.34,1.66) |
| | 2-m relative humidity (%) | 12.49 | 12.19 | -0.02[b] | (-0.08,0.03) |
| | 2-m vapor pressure deficit (kPa) | 1.921 | 1.952 | 0.02[b] | (-0.04,0.08) |
| | 10-m wind speed (m $s^{-1}$) | 22.19 | 22.33 | 0.01[b] | (-0.04,0.06) |
| CAd | 2-m temperature anomaly (°C) | -2.87 | -2.16 | **0.71**[a] | (0.37,1.06) |
| | 2-m relative humidity (%) | 10.37 | 10.36 | 0.00[b] | (-0.04,0.04) |
| | 2-m vapor pressure deficit (kPa) | 2.144 | 2.213 | 0.03[b] | (0.00,0.07) |
| | 10-m wind speed (m $s^{-1}$) | 32.75 | 33.15 | 0.01[b] | (0.00,0.03) |

[a]Difference: all forcings – natural forcings.
[b]Fractional difference: (all forcings – natural forcings) / natural forcings.
[a],[b]Bold-faced values have confidence intervals that do not include 0.
[c]95% confidence interval (C.I.)